Reversible high-pressure phase transition in LaN

Sebastian B. Schneider,[1] Dominik Baumann,[1] Ashkan Salamat,[2] and Wolfgang Schnick[1,a)]
[1]*Department Chemie, Ludwig-Maximilians-Universität, 81377 München, Germany*
[2]*European Synchrotron Radiation Facility (ESRF), 38000 Grenoble, France*

In situ high-pressure X-ray powder diffraction experiments on LaN up to 60.1 GPa at ambient temperature in a diamond-anvil cell revealed a reversible, first-order structural phase transition starting at ~22.8 GPa and completed at ~26.5 GPa from the ambient cubic phase ($Fm\bar{3}m$, no. 225) to a tetragonal high-pressure phase ($P4/nmm$, no. 19, $a = 4.1060(6)$, $c = 3.0446(6)$ Å, $Z = 2$, $wR_p = 0.011$), which has not been claimed in theoretical predictions. HP-LaN is isotypic with a high-pressure polymorph of BaO, which crystallizes in a tetragonally distorted CsCl-type structure. The phase transition is accompanied by a volume collapse of about 11% which corresponds well with the reported data on HP-BaO. A linear extrapolation of the c/a ratio of the tetragonally distorted CsCl-type sub-cell reaches a value $c/a = 1$ of cubic CsCl-type HP-LaN at 91(12) GPa. In addition, the compressibility of LaN was investigated and resulted in a bulk modulus for the ambient pressure phase of $B_0 = 135(3)$ GPa and $B' = 5.0(5)$ after fitting a third-order Birch-Murnaghan equation of state to the experimental p–V data. The corresponding extrapolated bulk modulus of HP-LaN is found to be $B_0 = 278(6)$ GPa and its pressure derivative $B' = 1.2(2)$. Both as-calculated bulk moduli are compared to the respective values obtained from an Eulerian strain versus normalized stress plot to be 143(2) GPa for ambient LaN and 293(7) GPa for HP-LaN. Compared to other binary nitrides such as δ-ZrN or δ-HfN having bulk moduli of 285 GPa and 306 GPa, respectively, the extrapolated bulk moduli of HP-LaN are in the same order of magnitude, ranking HP-LaN as a highly incompressible material. © *2012 American Institute of Physics.*
[http://dx.doi.org/10.1063/1.4709392]

I. INTRODUCTION

Recently, there has been extensive interest in scientific and technological application of rare earth mononitrides amongst which LaN in particular turned out to be very promising due to its unique optical, electronic, magnetic, mechanical, and vibrational properties related to its crystal structure.[1–8] As the high-temperature and ambient pressure structure for LaN is the well-known rocksalt structure type (B1) in space group $Fm\bar{3}m$ (no. 225), the high-pressure behavior of this compound attracted remarkable interest over the last few years.[2,3,6,9–12] In order to further study the exceptional properties of LaN at high-pressure conditions, pressure-induced structural phase transitions have been investigated theoretically. Thereby, a phase transition into the CsCl-type structure (B2) has been predicted at transition pressures of 25–100 GPa depending on the applied theoretical method. The corresponding calculated bulk moduli of B1 and the latter B2 phase range in between 121–173 GPa and 88–282 GPa, respectively. However, no experimental data confirming any of the theoretical predictions have been obtained so far. Recently, Hasegawa *et al.* succeeded in synthesizing two novel lanthanum nitrides with RE_2N_3 composition using laser heated diamond-anvil cells. However, they did not start with the mononitride itself, but with elemental lanthanum and nitrogen, the latter acting both as pressure transmitting medium and reacting agent.[13]

Here, we report on the first experimental *in situ* high-pressure data for LaN obtained with the diamond-anvil cell technique to verify the predicted B1–B2 phase transition. Therefore, the high-pressure structural evolution up to 60.1 GPa is reported. Additionally, the compressibility of LaN and an observed high-pressure polymorph, which is isotypic with a high-pressure phase of BaO[14–19] and homeotypic with Ph4X (X = Br, I),[20,21] is investigated by a third-order Birch-Murnaghan equation of state fitted to the obtained p–V data and compared to the values obtained from an Eulerian strain versus normalized stress $F(f)$-plot and to predicted values in the literature.[2,3,6,9–12]

II. EXPERIMENTAL DETAILS

A. *In situ* x-ray powder diffraction

In situ X-ray powder diffraction experiments at high pressure were carried out on beamline ID27 at the ESRF.[22] A membrane driven diamond-anvil cell equipped with 250-μm culet diamonds and a rhenium gasket was used with an automated pressure drive.[23] The gasket was pre-indented to 38 μm and a 120-μm hole working as a sample chamber was drilled into the gasket using a Nd:YAG laser. Nitrogen, N_2 (gas loading), served as the pressure transmitting medium (PTM). The sample (LaN, Alfa Aesar, 99.9%) was loaded onto a bedding of three ruby spheres. As LaN is extremely sensitive to moisture, the entire loading procedure had to be performed in an argon filled glove box. The pressure was determined by the ruby fluorescence scale according to the calibration (Ne) described by Mao *et al.*[24] For the high-pressure experiment,

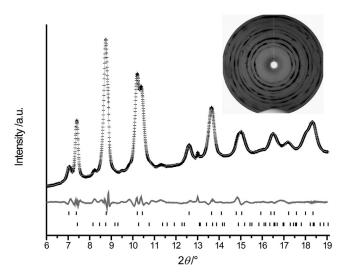a)Electronic mail: wolfgang.schnick@uni-muenchen.de.

FIG. 1. Observed (crosses) and calculated (gray line) diffraction pattern as well as difference profile of the Rietveld refinement of HP-LaN at 60.1 GPa; peak positions of HP-LaN (top) and ε-N_2 (bottom) are marked by vertical lines. Two-dimensional image plate data (upper right) were reduced and corrected (masking of diamond spots, dark gray) using the software FIT2D.

monochromatic radiation with a wavelength of $\lambda = 0.3738\,\text{Å}$ was selected. The beam was focused on a $3 \times 3\,\mu m^2$ area and a total number of 60 diffraction images were collected at pressures ranging from 1.3 to 60.1 GPa. The pressure at each diffraction image was measured before and after the data collection and averaged to its final value. Diffracted intensities were recorded with a MAR165 charge-coupled device detector. Exposure time was typically 5–20 s, depending on saturation of the detector. To average on texture and strain effects for selected images, the cell was oscillated in general by $\pm 10^\circ$ relative to the beam. A precise calibration of the detector parameters was performed with LaB_6 powder as reference material. The diffraction images were processed and integrated using the program FIT2D.[25] Individual single diffraction spots from the diamond anvils were masked manually and excluded from integration.

Indexing and Rietveld refinement for both phases was performed with the TOPAS package.[26] In case of LaN crystallizing in the B1-type structure, the crystallographic data at ambient conditions[27] were taken as starting values for stepwise Rietveld refinement up to higher pressures. The crystal structure of

TABLE I. Details of the Rietveld refinements and *in situ* crystallographic data for ambient LaN and HP-LaN at various pressures.

Compound		LaN		HP-LaN	
Pressure (GPa)		1.3(5)	19.7(5)	39.9(5)	60.1(5)
Structure type		NaCl		HP-BaO, (Refs. 14–19) PH_4X (X = Br, I) (Refs. 20 and 21)	
Space group		$Fm\bar{3}m$ (no. 225)		$P4/nmm$ (no. 129, origin1)	
a (Å)		5.2912(7)	5.1103(10)	4.1875(18)	4.1060(6)
c (Å)				3.1579(10)	3.0446(6)
V (Å^3)		148.14(6)	133.46(8)	55.37(5)	51.33(1)
Z		4	4	2	2
ρ (g/cm^3)		6.8557(1)	7.61(0)	9.1702(1)	9.8929(1)
Atom (site)					
La1 (4b)	x	$1/2$	$1/2$		
	y	$1/2$	$1/2$		
	z	$1/2$	$1/2$		
N1 (4a)	x	0	0		
	y	0	0		
	z	0	0		
La1 (2c)	x			0	0
	y			$1/2$	$1/2$
	z			0.3450(23)	0.3586(8)
N1 (2a)	x			0	0
	y			0	0
	z			0	0
2θ range ($^\circ$)		6–19		6–19	
Method of refinement		Fundamental parameter model		Fundamental parameter model	
Program package		TOPAS ACADEMIC		TOPAS ACADEMIC	
Atomic parameters		2		4	
Background function		Shifted Chebyshev		Shifted Chebyshev	
/parameters		8	8	12	12

HP-LaN was solved *ab initio* at 60.1 GPa (see Fig. 1). The indexing resulted unambiguously in a tetragonal unit cell with $a = 4.12$ and $c = 3.05$ Å. Integrated intensities were extracted using the Pawley-method.[28] The structure solution using the charge-flipping algorithm[29] yielded the complete structural model in space group *P4/nmm*.[30] Subsequently, the lattice and atomic parameters were refined using the Rietveld method. The reflection profiles were determined using the fundamental parameters approach[31] by convolution of appropriate source emission profiles with axial instrument contributions and crystalline microstructure effects. Preferred orientation of the crystallites was described with a spherical harmonics function of 8th order. A structural search within several databases with corresponding lattice parameters in the tetragonal crystal system showed that HP-LaN is isotypic with a high-pressure polymorph of BaO and homeotypic with PH_4X (X = Br, I) crystallizing in a tetragonally distorted CsCl-type structure. Depending on pressure, the corresponding HP-phases of nitrogen (δ- and ε-N_2)[32,33] have also been refined together with ambient or/and HP-LaN in order to obtain the correct lattice parameters upon Rietveld refinement of both LaN phases (see Table I). In between the starting and final pressure of transformation (22.8–26.5 GPa), both LaN phases were refined simultaneously. As the structure of HP-LaN was solved and refined at 60.1 GPa, these corresponding values were taken as starting values for the stepwise Rietveld refinement down to lower pressures.

Further information of the crystal structure of HP-LaN at 60.1 GPa (Ref. 33) may be obtained from the Fachinformationszentrum Karlsruhe on quoting the depository number CSD-423936.

B. Equation of state

The isothermal bulk moduli B_0 and their pressure derivatives B' for both LaN phases were analysed from fits of a third-order Birch–Murnaghan (BM) equation of state (EoS) (Refs. 34 and 35) to the obtained *p–V* data at 300 K with an error in pressure set to 0.5 GPa

$$p = 3B_0 f(1 + 2f)^{5/2} \times [1 + 3/2(B' - 4)f], \quad (1)$$

where

$$f = [(V/V_0)^{-2/3} - 1]/2, \quad (2)$$

represents the Eulerain strain, in which V_0 reflects the volume at zero pressure, so
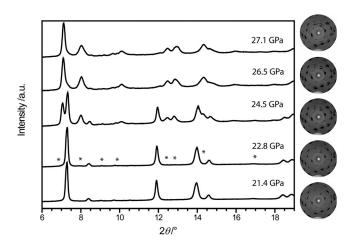

FIG. 2. Selected XRD images and patterns illustrating the phase transition from ambient to HP-LaN starting at 22.8 GPa (asterisks) and completed at 26.5 GPa.

$$p = 3/2B_0[(V/V_0)^{-7/3} - (V/V_0)^{-5/3}]$$
$$\times \{1 - 3/4(4 - B')[(V/V_0)^{-2/3} - 1)]\}. \quad (3)$$

For the ambient phase of LaN, the lattice parameters at zero pressure were taken from the *Pearson's Crystal Database*.[27] To obtain the lattice parameters at zero pressure for HP-LaN, the refined parameters at high pressures were extrapolated to zero pressure. Therefore, the bulk modulus and the first pressure derivative of HP-LaN refer to the extrapolated values to zero pressure. To check the quality of the EoS fit, the BM-EoS was also expressed in terms of the Eulerian strain *f* and the normalized pressure *F*, which is

$$F = p/3f(1 + 2f)^{5/2}. \quad (4)$$

The compression data are therefore additionally presented in a *F(f)*-plot,[36] where the intercept with the *F*-axis yields B_0, whereas the slope is $3 \times B_0(B' - 4)/2$ and thus provides B'.

$$F = B_0 + [3B_0(B' - 4)f]/2. \quad (5)$$

The *F(f)* form of representation of the *p–V* data is very sensitive to scattering of data and to experimental uncertainties as the bulk modulus and the first pressure derivative are obtained by a linear fit.[35] Both expressions of B_0 and B', the third-order BM-EoS fits and the *F(f)*-plot calculations were done using the software ORIGIN.[37]
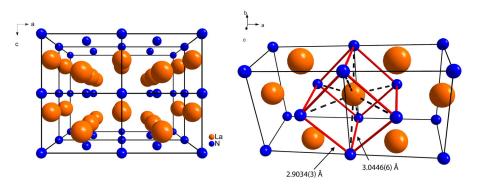

FIG. 3. $2 \times 2 \times 2$ super cell of HP-LaN at 60.1 GPa oriented along [101] (left) and doubled unit cell with illustration of the tetragonally distorted sub-cell of the CsCl-type structure indicated by continuous lines between the nitrogen atoms (right).
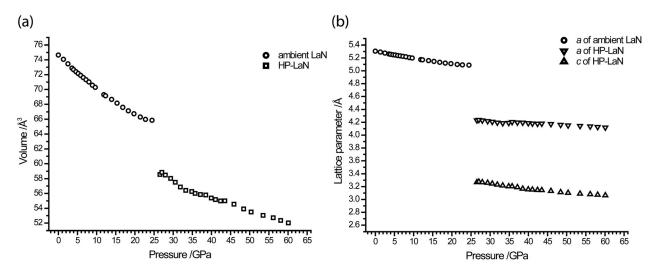
FIG. 4. (a) $V(p)$ plot of ambient and HP-LaN. The volume is given with respect to $Z=2$ to better compare the ambient ($Z=4$) to the high-pressure phase ($Z=2$). The volume collapse of about 11% clearly indicates a first-order phase transition. (b) Evolution of lattice parameters of both LaN phases with pressure.

III. RESULTS AND DISCUSSION

A. Phase transition and crystal structure of HP-LaN

Cubic B1-type LaN starts to transform into a tetragonal high-pressure polymorph at 22.8 GPa (see Fig. 2) in space group $P4/nmm$ (no. 129). The completion pressure of this reversible phase transformation is found to be 26.5 GPa. The high-pressure phase of LaN is isotypic with a high-pressure polymorph of BaO (stable above 15 GPa) and homeotypic with PH_4X (X = Br, I) crystallizing in a tetragonally distorted CsCl-type (see Fig. 3). After decompression, ambient LaN is recovered at 1.0 GPa. If the high-pressure behavior of LaN is compared with the structural sequence of BaO upon high-pressure, the intermediate NiAs-type structure of BaO
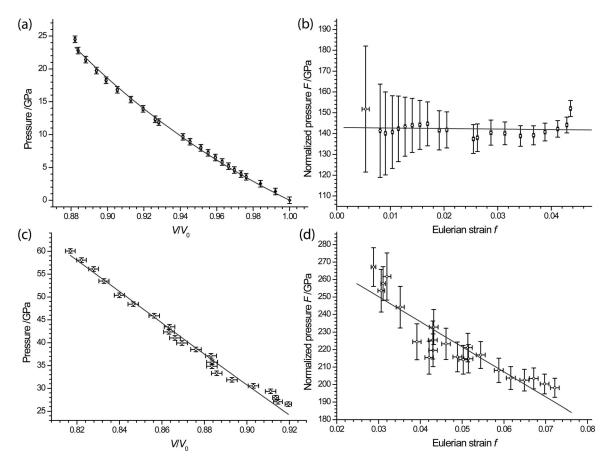

FIG. 5. (a) and (c) Third-order Birch-Murnaghan fits (gray line) to the experimental p–V data (left) of ambient LaN and HP-LaN. For HP-LaN, the volume at zero pressure (V_0) was obtained by extrapolation of the p–V data to ambient conditions and the first p–V data were taken at 26.5 GPa. (b) and (d) $F(f)$-plot with linear fits (gray line) to the applied values of the third-order BM-EoS of ambient LaN and HP-LaN. All fits are in fair agreement to the experimental data. The error in pressure is set to 0.5 GPa. Top: ambient LaN; bottom: HP-LaN.

forming at only 10 GPa has not been observed for LaN.[14–19] Additionally, this structure type has not been mentioned in the theoretical high-pressure predictions of LaN.[2,3,6,9–12] Accordingly, the B1-type structure transforms directly into the CsCl structure type at 25–100 GPa. For BaO, the B2 structure is found to be stable at a pressure of 60.5 GPa. This might indicate that at a pressure higher than 60.1 GPa another phase transformation from the tetragonally distorted into the cubic CsCl structure type is observable. This presumption is verified by a linear extrapolation of the c/a ratio of the tetragonally distorted CsCl-type sub-cell (see Fig. 3 continuous lines) which reaches a value $c/a = 1$ of cubic CsCl-type HP-LaN at 91(12) GPa.

The crystal structure of HP-LaN is built up of only two formula units per unit cell in contrast to ambient LaN with $Z = 4$. According to the (distorted) CsCl-type structure, the coordination number of both ions is 8 resulting in a (distorted) cubic coordination sphere (see Fig. 3).

Upon transformation from ambient cubic to tetragonal LaN, the volume drops by ~11% (see Fig. 4), clearly indicating a first-order phase transition. The extrapolated unit cell volume of HP-LaN at ambient pressure is smaller by about 14.7% compared with that of ambient LaN. This is quite reasonable considering the difference in volume at the phase transition.

B. EoS analysis

Fits of a third-order Birch-Murnaghan equation of state to the experimental p–V data are presented in Figs. 5(a) and 5(c). The corresponding linear fits of the $F(f)$-plot are illustrated in Figs. 5(b) and 5(d). To calculate the bulk modulus B_0 and the first pressure derivative of the high-pressure phase of LaN, the p–V data were extrapolated to zero pressure giving V_0, which was used as starting volume for the calculations. The results of all fits are summarized in Table II. Since the differences in B_0 and B' obtained from EoS analysis and the linear fit of the $F(f)$-plots are in the same range, the EoS fit can be considered of good quality. In addition, the obtained bulk moduli of ambient LaN do perfectly match the predicted values of 121–173 GPa.[2,3,6,9–12] The extrapolated

bulk moduli of HP-LaN with values of 278.5(6.4) and 293.2(7.2) GPa are extremely high, ranking HP-LaN as a highly incompressible material comparable to δ-ZrN or δ-HfN having bulk moduli of 285 GPa and 306 GPa, respectively.[38]

As expected, the high-pressure phase is less compressible than the ambient phase and shows a smaller first pressure derivative of the bulk modulus. This corresponds to the usually expected behavior as the repulsive forces of atoms become stronger at higher pressure. According to the sudden drop in volume at the phase transition, the bulk modulus increases.

IV. CONCLUSION

By *in situ* high-pressure experiments on LaN in a diamond-anvil cell, we were able to identify a reversible, first-order phase transition from the ambient cubic phase to a tetragonally distorted CsCl-type structure, which was not considered in recent theoretical predictions. Therefore, to properly predict the high-pressure behavior of LaN, the high-pressure phase has to be taken into account. HP-LaN is isotypic with a high-pressure polymorph of BaO undergoing a final phase transition into the B2-type structure at pressures higher than 60 GPa. In this context, we experimentally predict another phase transition to the cubic CsCl-type phase at a pressure of 91(12) GPa. Furthermore, this observation matches the theoretical predicted pressure range for a B1–B2 transition. Additionally, the compressibility was analyzed for both phases. For ambient LaN, the obtained bulk moduli perfectly match the predicted values. For HP-LaN, the bulk moduli range in between those of δ-ZrN or δ-HfN which ranks HP-LaN a highly incompressible material.

TABLE II. Bulk moduli B_0 and first pressure derivatives B' of ambient LaN and HP-LaN calculated by a third-order Birch-Murnaghan EoS and normalized strain fits to the experimental p–V data.

	BM 3rd	Nat. Strain 3rd
Ambient LaN		
a_0 (Å)		5.305
V_0 (Å^3)		149.3
B_0 (GPa)	135.5(3.5)	142.9(1.8)
B'	5.0(5)	3.9(2)
HP-LaN		
a_0 (Å)		4.3169(30)
c_0 (Å)		3.4424(31)
V_0 (Å^3)		63.68(1)
B_0 (GPa)	278.5(6.4)	293.2(7.2)
B'	1.2(2)	0.7(2)

[1]V. A. Gubanov, A. L. Ianovsky, and V. P. Zhukov, in *Electronic Structure of Refractory Carbides and Nitrides* (Cambridge University Press, Cambridge, 1994).
[2]Y. O. Ciftci, K. Colakoglu, E. Deligoz, and H. Ozisik, Mater. Chem. Phys. **108**, 120 (2008).
[3]G. Vaitheeswaran, V. Kanchana, and M. Rajagopalan, Solid State Commun. **124**, 97 (2002).
[4]F. Hulliger, J. Magn. Magn. Mater. **8**, 183 (1978).
[5]K. A. Gschneider, Jr., and I. R. Eyring, in *Handbook of Physics and Chemistry of Rare Earths* (North Holland, Amsterdam, 1974), Vol. 4, p. 153.
[6]C. Stampfl, W. Mannstadt, R. Asahi, and A. J. Freeman, Phys. Rev. B **63**, 155106 (2001).
[7]R. Norman, H. J. F. Jansen, D. D. Koelling, and A. J. Freeman, Solid State Commun. **52**, 739 (1984).
[8]A. Hasegawa, J. Phys. C **13**, 6147 (1980).
[9]D. R. Hamann, X. Wu, K. M. Rabe, and D. Vanderbilt, Phys. Rev. B **71**, 035117 (2005).
[10]A. Rukmangad, M. Aynyas, and S. P. Sanyal, Indian J. Pure Appl. Phys. **47**, 114 (2009).
[11]M. Ghezali, B. Amrani, Y. Cherchab, and N. Sekkal, Mater. Chem. Phys. **112**, 774 (2008).
[12]S. D. Gupta, S. K. Gupta, and P. K. Jha, Comput. Mater. Sci. **49**, 910 (2010).

[13]M. Hasegawa, K. Nivwa, and T. Yagi, Solid State Commun. **141**, 267 (2007).

[14]L.-G. Liu, J. Appl. Phys. **42**, 3702 (1971).

[15]L.-G. Liu and W. A. Bassett, J. Geophys. Res. **77**, 4934, doi:10.1029/JB077i026p04934 (1972).

[16]M. Uludoğan, T. Çağin, A. Strachan, and W. A. Goddard III, J. Comput.-Aided Mater. Des. **8**, 193 (2001).

[17]R. G. Amorim, M. Verissimo-Alves, and J. P. Rino, Comput. Mater. Sci. **37**, 349 (2006).

[18]S. T. Weir, Y. K. Vohra, and A. L. Ruoff, Phys. Rev. B: Condens. Matter **33**, 4221 (1986).

[19]I. Lukačević, Phys. Status Solidi B **248**, 1405 (2011).

[20]A. Sequeira and W. C. Hamilton, J. Chem. Phys. **47**, 1818 (1967).

[21]L. W. Schroeder and J. J. Rush, J. Chem. Phys. **54**, 1968 (1971).

[22]M. Mezouar *et al.*, J. Synchrotron Radiat. **12**, 659 (2005).

[23]R. Letoullec, J. P. Pinceaux, and P. Loubeyre, High Press. Res. **1**, 77 (1988).

[24]H.-K. Mao, J. Xu, and M. J. Bell, Geophys. Res. **91**, 4673, doi:10.1029/JB091iB05p04673 (1986).

[25]A. P. Hammersley, S. O. Svensson, M. Hanfland, A. N. Fitch, and D. Hausermann, High Press. Res. **14**, 235 (1996).

[26]A.A. Coelho, *TOPAS-Academic*, Version 4.1, Coelho Software, Brisbane, 2007.

[27]P. Villars, and K. Cenzual, *Pearson's Crystal Data—Crystal Structure Database for Inorganic Compounds*, Version 1.3d (ASM International, Ohio, 2009/2010).

[28]G. S. Pawley, J. Appl. Crystallogr. **14**, 357 (1981).

[29]G. Oszlányi and A. Sütő, Acta Crystallogr., Sect. A: Found. Crystallogr. **60**, 134 (2004); G. Oszlányi and A. Sütő, *ibid*. **64**, 123 (2008); A. A. Coelho, *ibid*. **63**, 400 (2007).

[30]Crystal data for HP-LaN at 60.1 GPa: formula: LaN, $M = 152.92$ g mol^{-1}, space group $P4/nmm$ (no. 129, origin1), $a = 4.1060(6)$, $c = 3.0446(6)$ Å, $V = 51.33(1)$Å^3, $Z = 2$, radiation: $\lambda = 0.3738$ Å, $T = 298(2)$ K, 17 reflections, 17 parameters, $R_p = 0.0080$, $wR_p = 0.011$, $\chi^2 = 1.182$, $R_{bragg} = 0.0768$, background: shifted Chebychev, 12 background parameters. Further information of the crystal structure of HP-LaN at 60.1 GPa can be obtained from Fachinformationszentrum Karlsruhe, 76344 Eggenstein-Leopoldshafen, Germany (fax: (49) 7247–808–666; e-mail: crysdata@fiz-karlsruhe.de).

[31]J. Bergmann, R. Kleeberg, A. Haase, and B. Breidenstein, Mater. Sci. Forum **347–349**, 303 (2000).

[32]E. Gregoryanz, A. F. Goncharov, C. Sanloup, M. Somayazulu, H.-K. Mao, and R. J. Hemley, J. Chem. Phys. **126**, 184505 (2007).

[33]D. T. Cromer, R. L. Mills, D. Schiferl, and L. A. Schwalbe, Acta Crystallogr. B **37**, 8 (1981).

[34]F. Birch, Phys. Rev. **71**, 809 (1947).

[35]F. Murnaghan, Proc. Natl. Acad. Sci. USA **30**, 244 (1944).

[36]D. L. Heinz and R. Jeanloz, J. Appl. Phys. **55**, 885 (1984).

[37]Origin 6.1, v6.1052 (B232), OriginLab Corporation, 2000.

[38]X.-J. Chen, V. V. Struzhkin, Z. Wu, M. Somayazulu, J. Qian, S. Kung, A. N. Christensen, Y. Zhao, R. E. Cohen, H.-K. Mao, and R. J. Hemley, Proc. Natl. Acad. Sci. U.S.A. **102**, 3198 (2005).